

## SESSION II—ELECTRONS IN NARROW BANDS

## Anomalous Transport Phenomena in Eu-Chalcogenide Alloys

T. KASUYA, A. YANASE

*Department of Physics, Tohoku University, Sendai, Japan*

Various anomalous optical, magnetic, and transport phenomena have been found in Eu-chalcogenide alloys. Anomalous optical properties are explained by the magnetic exciton in which a hole in the 4*f* conduction band and an electron (for optically active magnetic exciton) in the 5*d* conduction band make a bound state. Strong *d-f* exchange interaction between the magnetic-exciton electron of 5*d* character and the 4*f* electrons in the surrounding Eu<sup>2+</sup> ions is the origin of the anomaly. Anomalous magnetic properties in dilute R<sup>3+</sup> alloys are explained by the properties of the giant spin molecule which comes from the strong *s-f* exchange interaction between the impurity electron and the 4*f* electrons at the central R<sup>3+</sup> and the surrounding Eu<sup>2+</sup>. The anomalous transition from the hopping type to the metallic-impurity band conduction in dilute R<sup>3+</sup> alloys is also explained by the temperature dependence of the activation energy due to the *s-f* exchange interaction in the magnetic-impurity state.

### I. INTRODUCTION AND REVIEW OF EXPERIMENTS

Among various rare-earth chalcogenide compounds, the series of the type RX, in which R means a rare-earth atom and X means O, S, Se, or Te, has been investigated fairly well due to many interesting properties. The recent experimental investigation of this series have been done mostly by the IBM group in Yorktown Heights and the Busch group in Zürich.<sup>1-37</sup>

In this series of compounds, Eu, Sm, and Yb usually prefer divalency and thus the compounds in which R is one of these are fairly good ionic crystals. The crystal structure of these compounds is the rock-salt type, and the lattice parameters are given by the sum of the ionic radius of each ion as shown in Table I, in which Eu compounds are shown as typical examples.

Other rare-earth atoms prefer trivalency. In the compounds of R<sup>3+</sup>, also, however, the rock-salt-type structure persists. Furthermore, R<sup>3+</sup>X and R<sup>2+</sup>X mix completely in the whole composition ratio with the same crystal structure. Therefore it seems natural to assume that in these compounds, also, the main bonding mechanism is of the ionic type. Then one excess electron enters in the conduction bands, which are formed mostly by the 6*s* and 5*d* states on the rare-earth site, and the usual metallic conduction appears as is observed experimentally. Then the atomic distance shrinks from the pure ionic one due to this metallic-bonding effect. In Table I, the cases for Gd and La compounds are also given as the typical examples of the trivalence magnetic and nonmagnetic

compounds, respectively. In the following we treat mostly Eu, Gd, and La compounds as typical examples.

It is interesting that the mixed compound R<sub>x</sub><sup>3+</sup>R<sub>1-x</sub><sup>2+</sup>X exists in the whole range 0 < *x* < 1, and changes from nonmetal to metal with increasing *x*. In Fig. 1, the change of the lattice parameter of the mixture Gd<sub>x</sub>Eu<sub>1-x</sub>Se is shown.<sup>32,33</sup> This shows that the metallic-bonding effect becomes important around *x* = 0.25 and the lattice parameter decreases rather sharply around this composition. The change of the conduction mechanism from the nonmetallic to the metallic is, however, more complicated. For very small *x*, a Gd atom enters in Eu<sup>2+</sup>Se<sup>2-</sup> as an impurity atom dilutely and an excess electron is trapped around Gd<sup>3+</sup>. This is similar to the usual impurity state in nonmagnetic semiconductors such as Ge, Si, or InSb, etc., but has much more complicated properties mainly due to the *s-f* exchange interaction with the 4*f* electrons on the central Gd<sup>3+</sup> and the surrounding Eu<sup>2+</sup>. Hereafter this is called the magnetic impurity state. Actually, very interesting magnetic properties are observed on these mixtures. In Fig. 1, the typical examples for Gd<sub>x</sub>Eu<sub>1-x</sub>Se and La<sub>x</sub>Eu<sub>1-x</sub>Se are given. The paramagnetic Curie temperature *θ* increases very rapidly with the initial increasing of *x* while the Curie temperature *T*<sub>c</sub> increases rather gradually. Actually, this phenomenon is explained by the properties of the magnetic impurity state. As *x* increases, the magnetic-impurity band is formed and this impurity band is merged into the conduction band of EuSe at about *x* = 0.25. This merging of the impurity band into the conduction bands corresponds to the appearance

TABLE I. The atomic distances and the ionic radii of RX and rare-earth metals.

	$N_R^a$ $\times 10^{22}/\text{cc}$	Atomic distance ( $\text{\AA}$ )		Sum of the ionic <sup>b</sup> radii ( $\text{\AA}$ )
		R-R	R-X	
EuO	2.95	3.63	2.57	2.51
EuS	1.89	4.21	2.98	2.93
EuSe	1.69	4.38	3.10	3.10
EuTe	1.39	4.67	3.30	3.30
Eu (bcc)	2.05	3.99	...	...
GdSe	2.07	4.09	2.89	3.02
Gd (hcp)	3.04	3.63	...	...
LaSe	1.80	4.29	3.03	3.13
La (dhcp)	2.67	3.74	...	...

<sup>a</sup> The number of R.  
<sup>b</sup> The following values of the ionic radii are used:  $\text{Eu}^{2+}$ , 1.19;  $\text{Gd}^{3+}$ , 1.11;  $\text{La}^{3+}$ , 1.22;  $\text{O}^{2-}$ , 1.32;  $\text{S}^{2-}$ , 1.74;  $\text{Se}^{2-}$ , 1.91;  $\text{Te}^{2-}$ , 2.11.

of the metallic bonding and the sharp decreasing of the lattice parameter mentioned before. The more detailed treatment of these phenomena is given in Sec. III.

Before the impurity band is merged into the conduction bands, the metallic-type impurity band conduction occurs for the range of much smaller  $x$ . Due to the complicated properties of the magnetic impurity state, however, the mechanism of the impurity band conduction is much more complicated and interesting than that of the usual semiconductor. In Figs. 2 and 3, the temperature dependence of the electrical resistivities for  $\text{La}_x\text{Eu}_{1-x}\text{S}$  and  $\text{Gd}_x\text{Eu}_{1-x}\text{Se}$  for small  $x$  are given.<sup>36,37</sup> When the temperature is much higher

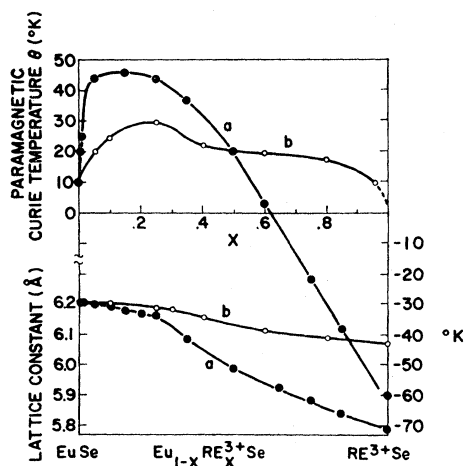


FIG. 1. Variation of the paramagnetic Curie temperature and the lattice constant of EuSe with  $\text{R}^{3+}$  substitution: (a)  $\text{Eu}_{1-x}\text{Gd}_x\text{Se}$ ; (b)  $\text{Eu}_{1-x}\text{La}_x\text{Se}$  (Holtzberg *et al.*<sup>32</sup>).

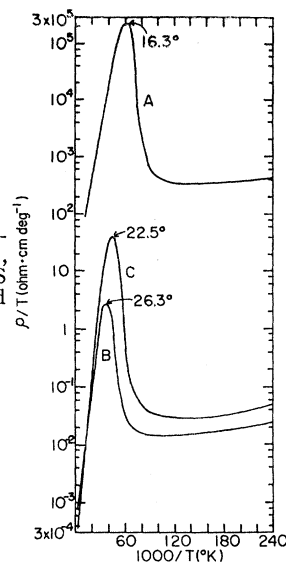


FIG. 2. The (resistivity/temperature) of  $\text{La}_{0.01}\text{Eu}_{0.99}\text{S}$  (A),  $\text{La}_{0.05}\text{Eu}_{0.95}\text{S}$  (B), and  $\text{La}_{0.1}\text{Eu}_{0.9}\text{S}$  (C) against  $1/T$  (Heikes and Chen<sup>36</sup>).

than room temperature, the impurity electrons are excited thermally into the conduction band and the electrical conductivity in the conduction band is dominant. This is shown in Fig. 4.<sup>38</sup> Below room temperature, the main conduction mechanism becomes the hopping-type impurity conduction similar to the usual semiconductor. The most drastic difference of the present case from the usual case is the sharp and very large decreasing of the resistivity around  $T_c$ , and below  $T_c$  the activation energy seems to disappear. Anomalous large negative magnetoresistance

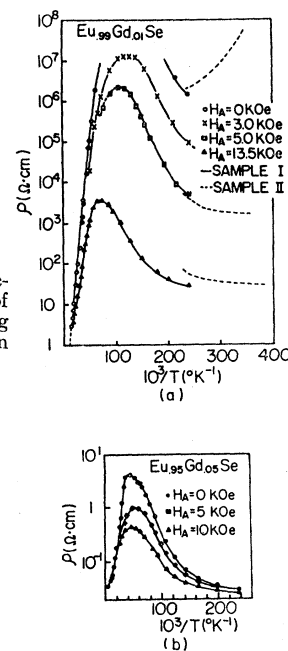


FIG. 3. Resistivity  $\rho$  of single-crystal  $\text{Eu}_{1-x}\text{Gd}_x\text{Se}$  as a function of reciprocal temperature at varying applied field strength  $H_A$  (von Molnar and Methfessel<sup>37</sup>).

TABLE II. The magnetic properties of RX.

	Spin structure <sup>a</sup>	Curie or Néel temperature (°K) <sup>c</sup>	Paramagnetic Curie temperature (°K) <sup>c</sup>	Exchange constant <sup>d</sup>		
				Nearest	Next nearest	Total $J^e$
EuO	Ferro	77	80	1.33	-0.12	15.2
EuS	Ferro	16.2	19	0.38	-0.16	3.62
EuSe	Screw <sup>b</sup>	4.6	8	0.25	-0.24	1.52
EuTe	Antiferro	9.6	-6	0.06	-0.31	-1.14

<sup>a</sup> Determined by neutron diffraction except EuS.<sup>b</sup> The complicated structure. See the text.<sup>c</sup> References 1-12 and 20-30.<sup>d</sup> Exchange energy is given by Eq. (5), in the unit of the Boltzmann constant.<sup>e</sup> The definition of  $J$  is given in Eq. (11a).

is also observed, as is shown in Fig. 3. These anomalous phenomena are also explained by the unusual properties of the magnetic impurity state as follows. The activation energy is caused now mostly as a result of the  $s$ - $f$  exchange interaction and then it depends strongly on temperature and magnetic field. It decreases sharply as the temperature decreases near  $T_c$  or when a strong magnetic field is applied, and then the conduction mechanism changes from the hopping-type to the metallic-type impurity band conduction. The more detailed treatment is given in Sec. IV.

The anomalous optical properties are also remarkable for these compounds. Actually the main interest of the IBM and Busch groups was initially in the optical properties. In Fig. 5, the absorption and the Faraday rotation are given for Eu compounds.<sup>28</sup> The large Faraday rotation indicates a magnetic transition. Further, it is observed that the absorption edge depends strongly on temperature and magnetic field.<sup>25,27,29</sup> The similar behavior is also observed for the emission spectrum as is shown in Fig. 6.<sup>26</sup> These

phenomena are explained in Sec. II by the magnetic-excitation model in which a hole is created in a  $4f$  level and an electron is excited onto the conduction band, and where the electron and hole make a bound state. It is interesting that the magnetic excitation is very similar to the magnetic impurity state. Actually,  $\text{Eu}^{3+}$  in the former corresponds to  $\text{Gd}^{3+}$  in the latter. Therefore the former information is very helpful for the understanding of the latter. In Sec. II, the model of the energy levels is proposed based on the various experiments.

Finally the magnetic properties of pure EuX compounds are reviewed very briefly. EuO and EuS are considered as typical examples of the insulator ferromagnet in which the Heisenberg exchange model is applicable, and various experimental and theoretical works have been done on these materials.<sup>7,13,15,16,18,19,21,22,38</sup> Yet, EuTe is a typical antiferromagnetic material.<sup>6,12,23</sup>

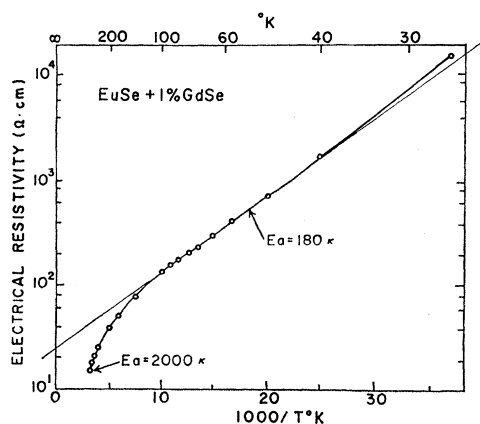


FIG. 4. Resistivity of  $\text{Eu}_{0.99}\text{Gd}_{0.01}\text{Se}$  as a function of reciprocal temperature (Methfessel<sup>33</sup>). Note the difference between this figure and Fig. 3, which should come from the difference in the degree of compensation.

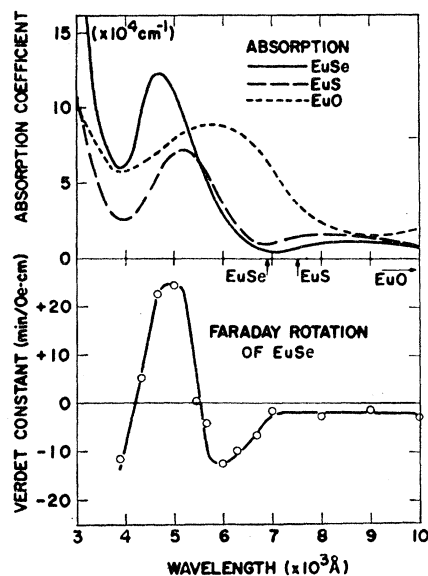


FIG. 5. Absorption and Faraday-rotation data for europium chalcogenide films at room temperature (Suits and Argyle<sup>28</sup>).

On the other hand, EuSe shows a complicated magnetic behavior because the ferromagnetic and the antiferromagnetic interactions are nearly the same order of magnitude.<sup>2,3,17</sup> It is believed that in EuSe the first transition occurs from the paramagnetic state to a screw-type structure and then to a state with ferromagnetic moment.<sup>4,5,10,11,27</sup> In Table II, various magnetic data are summarized.

## II. MODEL AND ENERGY LEVELS

Figure 7 shows a schematic picture of the energy levels of EuX in the sense of the Hartree-Fock approximation together with the exciton and the impurity state levels. This model is different essentially from the result of the band calculation by Cho.<sup>39</sup> The main different points of the band calculation are as follows: (1) The occupied  $4f$  levels are much lower than the  $4p$  valence bands and the unoccupied  $4f$  levels are just below the bottom of the conduction band. (2) The bottoms of the conduction band are at  $X_3$  and mostly formed by  $5d$  characters. The bottom of the  $6s$  band at  $\Gamma_1$  is about 2 eV higher than that at  $X_3$ . (3) The energy gap between the conduction and the valence bands is rather narrow, i.e., about 1.5 eV. However, various experiments are contrary to Cho's model but consistent with the model in Fig. 7. These discrepancies seem to come from the fact that in Cho's band calculation, the screening (or the correlation) effect is not taken into account, which is especially important for the ionic crystal and makes the band calculation of the ionic crystal very difficult. In fact, this effect has a tendency particularly to push down  $p$ -valence bands and the  $6s$ -conduction band and change the situation into Fig. 7 (see Appendix).

On the magnetic-exciton model, the temperature-dependent shift of the absorption edge or the emission edge should be due to the  $d$ - $f$  exchange inter-

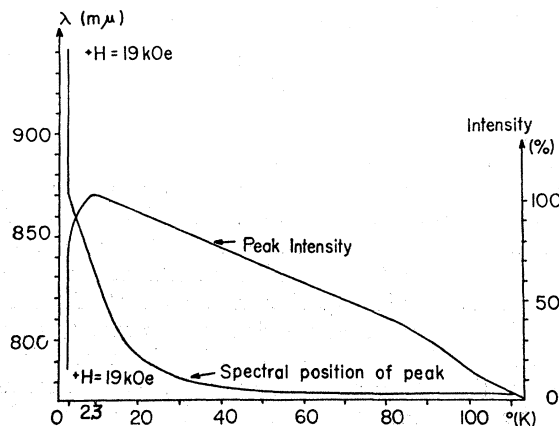


FIG. 6. Spectral position and intensity of the emission peak in EuSe as function of temperature (Busch and Wachter<sup>26</sup>).

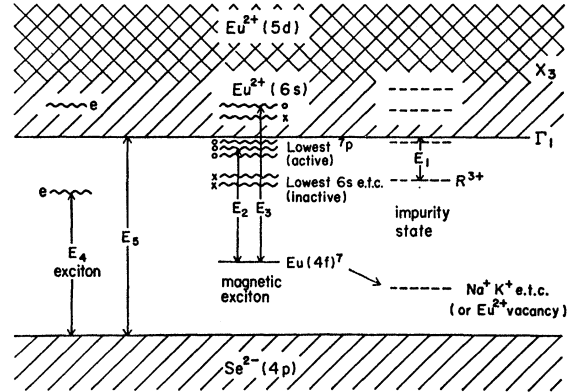


FIG. 7. Schematic picture of various energy levels in EuX together with the exciton and the impurity state levels.

action between the magnetic-exciton electron and the  $4f$  electrons except on the central Eu atom. Note that this magnetic exciton, as the hole is at a  $4f$  level, cannot move but is static. Also, the optically active magnetic-exciton electron should have  $d$  symmetry or  ${}^7P$  symmetry together with a  $4f$  hole, and then it is expected to be formed mostly by the  $5d$ -character bands located at  $X_3$ . The lowest-energy magnetic exciton with  $s$  character should be formed mostly by the  $6s$  band located at  $\Gamma_1$  but this is optically inactive. At the paramagnetic state the magnetic exciton has no energy gain of the  $d$ - $f$  exchange but at the ferromagnetic state it has full gain and the absorption edge shifts to the lower-energy side. Therefore, from the difference between the edge at the paramagnetic state and that at the ferromagnetic state, the magnitude of the  $d$ - $f$  exchange interaction is estimated as follows:

$$\begin{aligned} I_d &= \sum_n' J_{in}^d = 357 \text{ cm}^{-1} \quad (\text{absorption}^{29} \text{ for EuSe}), \\ &= 461 \text{ cm}^{-1} \quad (\text{absorption}^{27} \text{ for EuS}), \\ &= 657 \text{ cm}^{-1} \quad (\text{emission}^{26} \text{ for EuSe}), \quad (1) \end{aligned}$$

in which  $\sum_n'$  means to sum up by  $n$  except the center, and the  $d$ - $f$  exchange interaction is put as

$$\mathcal{H}_{df} = -2 \sum_n' J_{in}^d \mathbf{d}_i \cdot \mathbf{S}_n, \quad (2)$$

in which  $\mathbf{d}_i$  and  $\mathbf{S}_n$  are the spin operators of the magnetic-exciton electron and the  $4f$  electrons of  $\text{Eu}^{2+}$  at the  $n$ th site.

By comparing the emission data in Eq. (1) with the  $d$ - $f$  exchange constant in atomic  $\text{Eu}^{2+}$  listed in Table III,<sup>40,41</sup> it is estimated roughly that about 80% of the magnetic-exciton electron is outside of the central Eu atom. Corresponding to this large charge transfer, a large lattice distortion, mostly expected on the nearest-neighbor (n.n.)  $\text{X}^{2-}$  ions, is also ex-

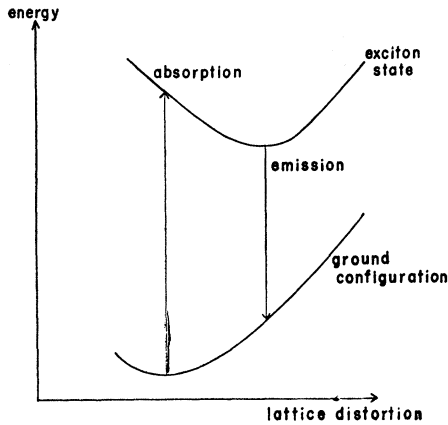


FIG. 8. Schematic picture for absorption and emission.

pected. This is observed as the large difference between the absorption and emission peaks; for example, about  $6000 \text{ cm}^{-1}$  in EuSe. Because the lattice distortion cannot follow the absorption and emission processes with such a large distortion energy, the emission process occurs under the distorted stable lattice position for the metastable magnetic exciton as is shown schematically in Fig. 8. The difference of the  $d$ - $f$  exchange energy in Eq. (1) between the emission and the absorption processes is also explained such that, for the distorted stable lattice position in which the nearest-neighbor  $X^{2-}$  ions shrink to the center, the wave function of the metastable magnetic-exciton electron spreads more to the outside.

The magnetic impurity state is similar to the magnetic exciton except that  $\text{Gd}^{3+}$  replaces  $\text{Eu}^{3+}$  at the center and now the lowest state formed by the  $6s$  band is most important. The main difference is that the  $s$ - $f$  exchange constant should be used instead of the  $d$ - $f$  exchange.

The binding energy of this impurity state is estimated from the electrical-conductivity<sup>38</sup> and the Hall-constant measurements<sup>37,42</sup> of  $\text{Gd}_{0.01}\text{Eu}_{0.99}\text{Se}$  at room temperature by the simple two-band analysis as follows:

$$E_1 = 6800\kappa, \quad (3)$$

and the mobility  $\mu_1$  and the number  $n_1$  of the electrons in the conduction band are also estimated as

$$\mu_1 = 1.1 \times 10^3 \text{ cm}^2/\text{V}\cdot\text{sec}, \quad n_1 = 5.7 \times 10^{14} \text{ cm}^{-3}, \quad (4)$$

at room temperature, in which the bottom of the conduction band is approximated by the free-electron model. Note the large mobility comparable to Ge and Si.<sup>43</sup> From the large binding energy  $E_1$ , which is more than one order of magnitude larger than the shallow levels in Ge and Si, and assuming the usual order of magnitude for the dielectric constant, i.e.,  $\epsilon \sim 10$ , the magnetic impurity state is expected to

extend mostly on the nearest-neighbor  $\text{Eu}^{2+}$  ion. (The detailed calculation is rather complicated because here the usual effective mass Hamiltonian is not applicable. However, roughly speaking, the occupation ratio is 2:6:2 for the central atom:the nearest-neighbor Eu atoms:the more outer space.) This is also consistent with the picture of the magnetic exciton investigated before.

From the above model, it is expected that the impurity-electron spin interacts strongly with  $4f$  electron spins at the center  $\text{R}^{3+}$  and at the nearest-neighbor  $\text{Eu}^{2+}$  through the  $s$ - $f$  exchange interaction. And, these spins are aligned parallel at low temperature and make a giant spin molecule. The study of the magnetic properties of this giant spin molecule is interesting in itself but also offers various important information for the impurity-state and the impurity-conduction mechanisms. In the next section, the giant spin molecule is treated in detail.

### III. GIANT SPIN MOLECULE

The effective spin Hamiltonian of the dilute  $\text{R}_x^{3+}\text{Eu}_{1-x}\text{X}$  system is given by

$$\mathcal{H}_{\text{ex}} = - \sum_{n>m} J_{nm} \mathbf{S}_n \mathbf{S}_m - 2 \sum_{i,n} J_{in} \delta_i \mathbf{S}_n - 4 \sum_{i>j} J_{ij} \delta_i \delta_j, \quad (5)$$

in which the first term means the direct-exchange interaction between  $4f$  electrons situated at the  $n$ th and  $m$ th lattice sites, the second term the  $s$ - $f$  exchange interaction between the  $i$ th impurity electron and the  $4f$  electrons at the  $n$ th site, and the third term the effective exchange interaction between the  $i$ th and  $j$ th impurity electrons. The values of  $J_{nm}$  are tabulated for pure samples in Table II.

First, the properties of an isolated spin molecule are considered. The effective spin Hamiltonian is now written as

$$\mathcal{H}_m = -2\delta(J_0 \mathbf{S}_c + J_1 \mathbf{S}_u), \quad (6)$$

in which  $\mathbf{S}_c$  is the spin of the central  $\text{R}^{3+}$  site and

$$\mathbf{S}_u = \sum_{n,n} \mathbf{S}_n \quad (7)$$

is the sum of the nearest-neighbor spins. Here the direct-exchange term is omitted because it is much smaller than the  $s$ - $f$  exchange interaction in the present compounds. This Hamiltonian is solved rigorously and in Figs. 9 and 10 some calculated results are shown for  $\text{R}^{3+} = \text{Gd}^{3+}$ . Similar results are obtained for a nonmagnetic impurity such as  $\text{La}^{3+}$ . It is remarkable that the effective giant spin moment, which is represented well by  $\chi_m T / (\chi_m T)_\infty$  because this is the effective Curie constant of the molecule normalized by the sum of the individual contribution, increases very rapidly as temperature decreases beyond  $J_1/\kappa$  and the peak of the specific heat also appears

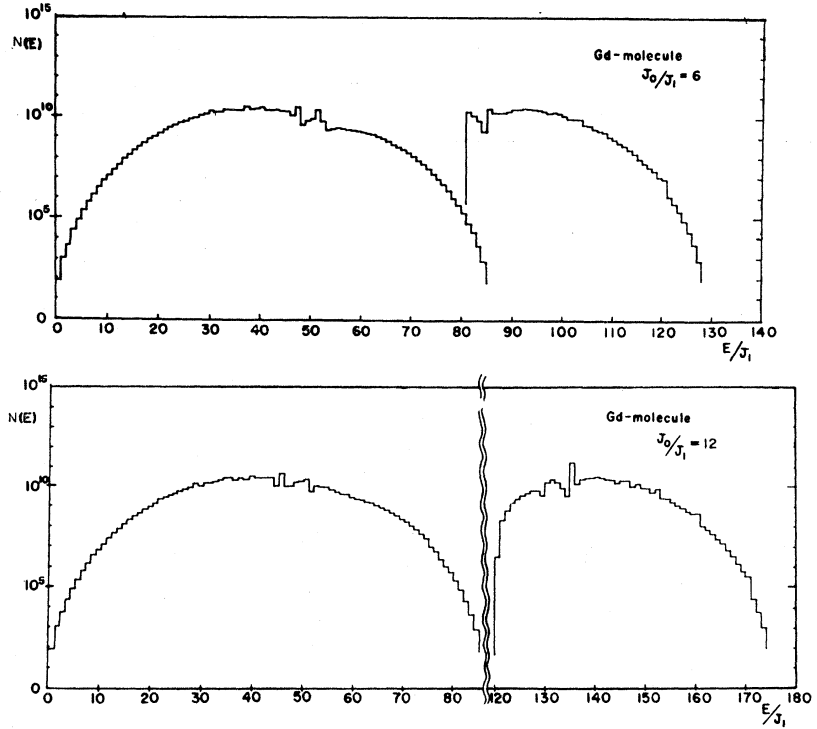


FIG. 9. Density of states of a Gd molecule as a function of the reduced energy  $E/J_1$ .

around  $\kappa T \sim J_1$ . This peak of the specific heat should be observed for a few percent of the  $R^{3+}$  alloys.<sup>44</sup>

To evaluate the experimental data of  $Gd_{0.01}Eu_{0.99}Se$ , for example, on the present model, the remaining terms in Eq. (5) should also be taken into account. This is done by the extended molecular-field model in which the total system is divided into molecules, and others called free Eu spins. Then the following equations are deduced:

$$\begin{aligned} \langle S \rangle &= \chi H_1, \\ \langle S_n \rangle &= \chi_n^n H_1 + \chi_n^0 H_2, \\ \langle \sigma \rangle &= \chi_0^n H_1 + \chi_0^0 H_2, \end{aligned} \quad (8)$$

in which

$$\begin{aligned} H_1 &= g\mu H + \phi J \langle S \rangle + xJ \langle S_n \rangle + xJ_2 \langle \sigma \rangle, \\ H_2 &= g\mu H + \phi J_2 \langle S \rangle + xJ_2 \langle S_n \rangle + I_{eff} \langle \sigma \rangle, \end{aligned} \quad (9)$$

$$S_n = S_u + S_c, \quad (10)$$

and  $S$  is a free Eu spin. Note that the definition of the susceptibility is different in the factor  $(g\mu)^2$  from the usual definition, and  $\chi_n^0$ ,  $\chi_0^n$ , etc., denote the spin susceptibility of  $S_n$  for the magnetic field applied on  $\sigma$ , etc., and  $\chi$  the spin susceptibility of an isolated  $Eu^{2+}$  spin. These values are calculated on the present model. Further,  $H$  is the external magnetic field,  $\phi = 1 - 13x$ ,  $x$  is the concentration of the

trivalent ion, and

$$J = \sum_m J_{nm}, \quad (11a)$$

$$J_2 = 2 \sum_n J_{in}, \quad (11b)$$

$$I_{eff} = 4 \sum_j J_{ij} + \Delta J_{sf}, \quad (11c)$$

in which  $J$  is known from the magnetic properties of pure  $EuX$ , and  $J_2$  is also roughly estimated on the present model using  $I_{sf}$  in Table III. Both  $J$  and  $J_2$  are positive, namely ferromagnetic, and  $J_2$  is much larger than  $J$ . For  $I_{eff}$ , the first term should be negative on the present model but positive on

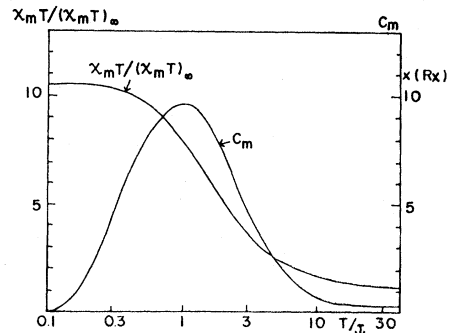


FIG. 10. Temperature dependence of the effective Curie constant  $\chi_m T$  and the specific heat  $C_m$  of a Gd molecule as a function of reduced temperature,  $T/J_1$ .

TABLE III. Exchange constant  $I_{ij}$  and the spin-orbit constant  $\lambda_i$  in units of  $\text{cm}^{-1}$ . Exchange is given by  $2I_{ij}\sigma_j$  and  $\sigma$  is the spin operator of the  $i$ th electron.<sup>a</sup>

	$I_{sf}$	$I_{pf}$	$I_{df}$	$\lambda_p$	$\lambda_d$
Eu <sup>+</sup>	209	114	787	1610	648
Gd <sup>2+</sup>	294	246	1013	3050	1050

<sup>a</sup> These values are obtained from the atomic spectrum data of Refs. 40 and 41.

the  $5d$  band model. The second term means the correction for the  $s$ - $f$  exchange energy when two molecules share some common nearest neighbor  $\text{R}^{3+}$ . Therefore this is not important for sufficiently separated molecules.

For the calculation of the paramagnetic Curie temperature  $\theta$ , only the values of  $\chi_{\text{tot}}$  near room temperature are necessary. Then, as the giant moment is reduced very much in the room-temperature region, both  $J_2$  and  $I_{\text{eff}}$  are not important, and the temperature dependence of the susceptibility of a molecule becomes most important. As  $\chi_m$  is the function of  $T/J_1$ ,  $J_1$  is determined as

$$J_1 = 25\kappa \quad \text{for } \text{Gd}_{0.01}\text{Eu}_{0.99}\text{Se},$$

or summed up on the nearest neighbor

$$12J_1 = 300\kappa = 209 \text{ cm}^{-1}.$$

This is, incidentally, equal to  $I_{sf}$  but much smaller than  $I_d$  in Eq. (1), and thus is consistent with the present model in that the impurity state is formed mostly by a  $6s$  band and located mostly on the nearest-neighbor Eu ions. The value of  $J_1$  is expected to be nearly equal in other Eu-chalcogenides alloys although there are no available experiments.

Next the ferromagnetic Curie temperature  $T_c$  is calculated. As  $T_c$  is lower than  $J_1$  in S, Se, and Te compounds, the giant moment near  $T_c$  is almost at its full value. Then the situation becomes similar to the usual superparamagnetism and both  $J_2$  and  $I_{\text{eff}}$  become important. Then, if both  $J_2$  and  $I_{\text{eff}}$  are positive, a large increase in  $T_c$  is expected. Experimentally, however,  $\Delta T_c$  is very small; for example,  $\Delta T_c/\Delta\theta = 0.13$  in  $\text{Gd}_{0.01}\text{Eu}_{0.99}\text{Se}$ .<sup>32</sup> This fact actually means that  $I_{\text{eff}}$  should be negative and nearly cancels the effect of  $J_2$ . The ratio of  $I_{\text{eff}}/J_2$  is determined from the experiment as about 9.<sup>42</sup> However, there is a fairly large ambiguity about the magnitude of  $J_2$ . For  $\text{Gd}_{0.01}\text{Eu}_{0.99}\text{O}$ , since  $\kappa T_c$  is fairly larger than  $J_1$ ,  $\Delta T_c$  and  $\Delta\theta$  should not be very much different, as is observed experimentally.<sup>45</sup> Then we can get more detailed information on the magnitude of  $J_2$ , and  $J_2$  is estimated as about  $50$ – $100\kappa$  and  $I_{\text{eff}}$  is about  $450$ – $900\kappa$ . The ratio  $J_2/12J_1$  is about  $0.17$ – $0.33$ , which is actually expected from the present model of the impurity state because this should be

nearly equal to (occupation probability of the impurity electron outer than the n.n.)/(that on the n.n.). The magnitude of  $I_{\text{eff}}$  is also reasonable with that expected from the two effective hydrogen molecules in a medium with the dielectric constant  $\epsilon = 10$ . In the present stage, there are no sufficiently detailed experiments to determine the magnitude of  $J_0$ .

When the concentration  $x$  of  $\text{R}^{3+}$  increases, the probability that two  $\text{R}^{3+}$  are situated at the nearest neighbor of each other increases. Then, as the negative exchange interaction exceeds the positive  $s$ - $f$  exchange interaction, the ground state becomes singlet and the giant spin disappears. Therefore this kind of molecule has no contribution to both  $\Delta T_c$  and  $\Delta\theta$ . If three  $\text{R}^{3+}$  are situated together at the nearest neighbor, the ground state becomes the doublet and contributes to  $\Delta\theta$  and  $\Delta T_c$ , but has  $\frac{1}{3}$  the efficiency of the isolated molecule. Figure 11 shows the relation between  $\Delta\theta$  and the number of the isolated  $\text{R}^{3+}$  which has no other  $\text{R}^{3+}$  at the nearest neighbor. Actually, the correlation between these two curves is good. The discrepancy at higher  $x$  is also corrected by taking into account the above-mentioned three trivalent ion-molecules, etc., and thus the saturation of  $\Delta\theta$  is expected. Figure 11 also includes the two experimental points of  $\Delta T_c$  and the expected curve of  $\Delta T_c$ . Note the difference between the expected curves for  $\Delta\theta$  and  $\Delta T_c$ . For small  $x$ ,  $\Delta\theta$  is expected to be proportional to  $x$  because  $\Delta\theta$  is determined mainly by the temperature dependence of the susceptibility of the isolated molecule.  $\Delta T_c$  is determined by the competition between  $J_2$  and  $I_{\text{eff}}$  in which  $J_2$  is nearly independent of  $x$  but  $I_{\text{eff}}$  is a complicated function of  $x$  and  $T$ . When the dis-

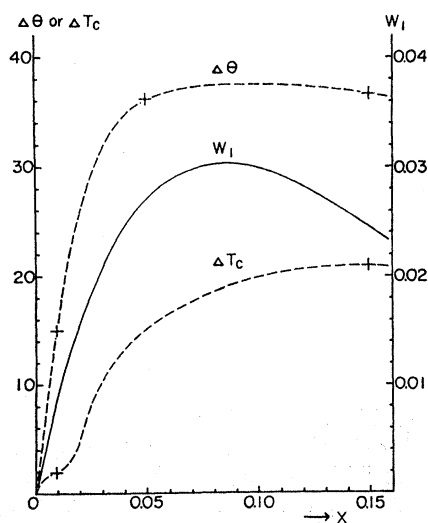


Fig. 11. The expected curves shown by dotted lines and the experimental values shown by + for  $\Delta\theta$  and  $\Delta T_c$  of  $\text{Gd}_x\text{Eu}_{1-x}\text{Se}$ . The probability  $w_1$  of the isolated molecule is also shown.

tance between two  $R^{3+}$  is sufficiently large, or  $x$  is less than 1%, and the temperature is near or higher than  $T_c$ ,  $I_{eff}$  is determined mostly by the usual exchange mechanism in a hydrogen molecule; that is, the first term in Eq. (11c). When the distance between two  $R^{3+}$  decreases and two impurity electrons share a common nearest neighbor, the positive  $s$ - $f$  exchange interaction of the second term of Eq. (11c) begins to contribute importantly to the effective exchange interaction between these two impurity states, and below the room temperature  $I_{ij}^{eff}$  is rather expected to be positive. This effect is expected to be important for  $x > 0.02$ , and then  $I_{eff}$  is expected to decrease in absolute magnitude as  $x$  increases from 0.01 to 0.02 and greater. The expected curve of  $\Delta T_c$  reflects this situation. Unfortunately, there are no available experiments. For the more detailed calculation of this section, see Ref. 42.

#### IV. MECHANISMS OF IMPURITY CONDUCTION

Here, the transport phenomena in  $Gd_{0.01}Eu_{0.99}Se$  are considered in detail.

Sufficiently above room temperature, the electrical transport occurs mostly in the conduction band. Below room temperature, however, the impurity conduction with the activation energy of about 200–300 $\mu$ eV is dominant.<sup>33,36,37</sup> The following three mechanisms are considered as the main possible sources of the activation energy.

##### A. The Local Potential Fluctuation Due to the Compensators and the Holes

This is the main origin of the activation energy for the most usual semiconductors such as Ge and Si.<sup>46</sup> The local-potential fluctuation is estimated by the following procedure by assuming that the compensation degree is sufficiently small.

First, the probability  $w_h$  that the nearest  $R^{3+}$  for a given compensator is located at the  $n$ th neighbor is calculated. This is also given as the function of the potential energy due to the compensator. For

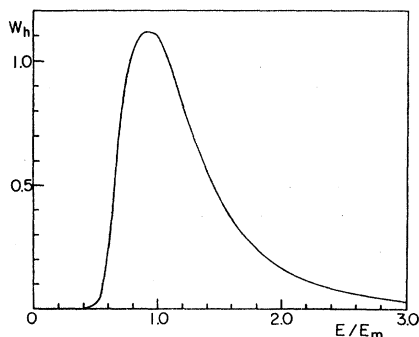


FIG. 12. The probability  $w_h$  as a function of the potential energy due to a given compensator.

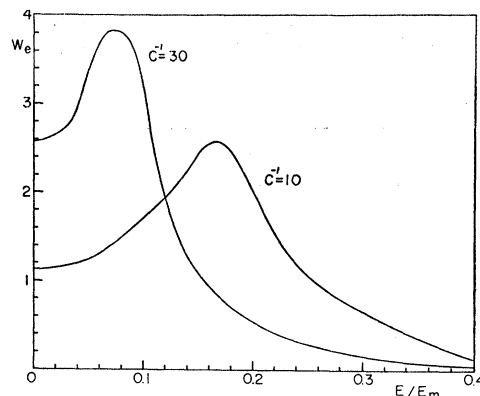


FIG. 13. The distribution  $w_e$  of the local-potential fluctuation due to the dipole field for the degree of the compensation  $C=1/10$  and  $1/30$ .

fairly large distances from the compensator, the continuous model is applicable for the lattice position, and then  $w_h$  is given by

$$w_h(\varepsilon) d\varepsilon = 3\varepsilon^{-4} \exp(-\varepsilon^{-3}) d\varepsilon, \quad (12)$$

in which

$$\varepsilon = E/E_m,$$

$$E_m = -e^2/\epsilon R_m,$$

$$N_m^{-1} = (4\pi/3) R_m^3, \quad (13)$$

and  $N_m$  is the number of  $R^{3+}$  per unit volume. This is shown in Fig. 12. Now the impurity electron on this  $R^{3+}$  is transferred onto the compensator and an effective hole appears around the  $R^{3+}$ . This is a bound hole, and this positive hole and the negative compensator make a molecule with electric dipole. Then  $E$  means the binding energy or the segregation energy of this bound hole. Note the sharp edge of the binding energy around  $\varepsilon=0.5$ .

For the transport phenomena, these bound holes should be segregated from the compensation and migrate through the crystal in which the local potential is created by the dipole molecules. The distribution of the dipole field is calculated also on the continuous model for a sphere of the volume  $N_c^{-1}$ , where  $N_c$  is the number of the compensator, in which the compensator and the bound hole are separated by the distance  $R_m$ . The distribution function  $w_e$  is given in Fig. 13 for  $1/C=10$  and  $30$ , where  $C=N_c/N_m$  is the degree of the compensation. The detailed structure has no meaning, but the following general tendency is seen that as  $C$  decreases the potential fluctuation becomes narrower and concentrates at zero energy. Actually, the width from the center is about  $\pm 0.2E_m$  for  $1/C=10$  and  $\pm 0.12E_m$  for  $1/C=30$ . When a bound hole segregates from the compensator, the segregation energy is smaller than the binding energy of the

TABLE IV. The overlapping integral  $J_c$  and the transfer energy  $U$  normalized by  $E_m$  for the critical distance.

$R_a/a$	$J_c$	$U_c/E_m$
3	0.61	0.555
4	0.40	0.364
5	0.27	0.246
6	0.18	0.164
7	0.11	0.100
8	0.07	0.064

isolated dipole molecule in Fig. 12 because of the screening effect due to other dipole molecules and impurity electrons. From this effect the edge of the segregation energy in Fig. 12 is roughly estimated to decrease to  $0.3E_m$  for  $1/C=10$  and  $0.4E_m$  for  $1/C=30$ . One-half of each of these values is the average activation energy  $\Delta E_a$ . For example, in  $R_{0.01}E_{0.99}X$  for  $1/C=10$ ,  $\Delta E_a$  is about  $220\kappa$ . Note that the effective  $\Delta E$  decreases with decreasing temperature because the hole prefers the path with low  $\Delta E$  particularly at low temperature.

As  $N_m$  increases, the overlapping energy, or the transfer energy, between two impurity states overcomes the local-potential fluctuation due to the dipole field, and then the metallic impurity band is formed. Note that the impurity band is different from the usual metallic band at the point where the impurity band is a strongly correlated band and at which only one electron can occupy one impurity site. It is difficult to determine the condition for the formation of the metallic impurity band in such a complicated system. Therefore, we estimate the condition very roughly as follows.

First, the probability  $w_d$  that the two sufficiently separated  $R^{3+}$  are linked by any path of  $R^{3+}$  in which the nearest distance is smaller than a given value  $d$  is defined. This is given by

$$-\ln(1-w_d)/w_d = (d/R_m)^3, \quad (14)$$

and  $w_d$  has a finite value only for  $d > R_m$ . Therefore  $d_c = R_m$  is the critical distance at which the path is formed with a finite probability. If the width of the local-potential fluctuation is restricted within a given value, the effective number of  $R^{3+}$  decreases correspondingly and  $d_c$  increases, or the transfer energy decreases. Table IV shows an example of the continuous lattice model. The potential fluctuation is restricted within a given value, the effective number of  $R^{3+}$  decreases correspondingly, and  $d_c$  increases, or the transfer energy decreases. Table IV shows an example of the continuous lattice model. The potential fluctuation is restricted to  $\pm 0.2E_m$  and then the effective

number of  $R^{3+}$  is about  $0.75N_m$  from Fig. 13. The overlap integral  $J_c$  and the transfer energy  $U_c$  are estimated for the effective hydrogen-molecule model separated by  $d_c$ . For simplicity,  $U_c$  is approximated by

$$U_c = (e^2/\epsilon d_c)J_c = (R_m/d_c)J_c E_m \quad (15)$$

and

$$(R_m/d_c) = (0.75)^{1/3} = 0.91. \quad (16)$$

In the present picture, the bandwidth due to the transfer energy is expected to be  $\pm 2U_c$ , and  $R_{0.01}^{3+}E_{0.99}X$  corresponds to about  $R_a/a=7$  for the continuous model in which  $R_a = N_m^{-3}$  and  $a$  is the effective Bohr radius. Then, the interesting thing is that, for  $R_a/a=7$ , the bandwidth and the local-potential fluctuation is just the same,  $\pm 0.2E_m$ . If this equality is considered as the criterion of the impurity-band formation, 1% trivalent alloy is just in the critical situation, and if  $x$  is smaller than 0.01, the impurity band may not be formed. The experiment with the nonmagnetic material such as  $R_x^{3+}Sr_{1-x}X$  is interesting at this point.

In summary, if the local-potential fluctuation is the only source of the activation energy, or in the nonmagnetic alloys, it is expected that, for  $x$  smaller than 0.01, the finite activation energy persists in the whole temperature range although it may decrease with decreasing temperature, and for  $x$  larger than 0.01 the impurity band is formed, and when any bound hole belongs to this band the metallic conduction without activation energy overcomes the hopping conduction at sufficiently low temperature. As  $x$  increases, the transition from the hopping-dominant region to the impurity-band-dominant region occurs at higher temperature. The complicated phenomena in the intermediate impurity concentration<sup>47</sup> found in Ge and Si seem to also occur from a similar situation.

## B. Activation Energy Due to the Electron-Phonon Interaction

When an impurity electron is localized at an  $R^{3+}$  site, the lattice distortion occurs in the same way as that shown in Fig. 8 corresponding to the charge transfer. When the impurity electron is transferred to another vacant site, the further lattice distortion is accompanied. If the lattice energy due to this further distortion is smaller than the typical optical phonon, this lattice distortion can follow the process of the electron transfer and no activation energy is observed.<sup>48</sup> For the reverse situation, it is hard for the lattice distortion to follow the electron transfer, and the activation energy should be observed at higher temperature. For EuX alloys, the lattice distortion energy is expected to be about  $3000\text{ cm}^{-1}$  for the first distortion. If it is assumed that the distortion energy is proportional to the square of the transferred charge and that the 80% charge transfer occurs

first, which comes from the fact that the impurity electron is located about 20% at the central  $R^{3+}$ , the lattice distortion energy accompanied by the transfer of the impurity electron to the other site is estimated roughly as  $200 \text{ cm}^{-1}$ . This is usually smaller than the optical phonon energy and thus no activation is expected from the present mechanism.

### C. Activation Energy Due to the s-f Exchange Interaction

Figure 9 shows the probability that a magnetic impurity state has a given energy  $E$ . The first peak comes from the ferromagnetic configuration of  $\delta$  and  $S_c$ , the spin of the central  $R^{3+}$ , and the second from the antiferromagnetic coupling. Even within the first configuration, the width is about  $80J_1=2000\kappa$ . Therefore the energy fluctuation in the magnetic impurity state due to the s-f exchange interaction is much larger than other energy fluctuations and masks others in most of the temperature range except for very high and very low temperatures.

The activation energy due to this energy fluctuation is strongly temperature dependent. For a much higher temperature than that for the s-f exchange energy, the activation energy tends to zero because the 4f spin ordering is at random for both occupied and unoccupied impurity sites. For a very low temperature in the ferromagnetic ordering phase, also, the activation energy tends to zero because the 4f spins are completely ordered everywhere. In the intermediate temperature range, the activation energy is finite and large because, in the occupied site, the 4f spins are aligned by the impurity-electron spin so as to gain the energy of the s-f exchange interaction, but no alignment of 4f spins in the unoccupied site, and thus the activation energy is required for the impurity electron to transfer from one site to another unoccupied site. The strong negative magnetoresistance in Fig. 2 is easily explained on the present picture because the increasing of the 4f spin alignment on the unoccupied site due to the applied magnetic field is much larger than that on the occupied site so that the effective activation energy decreases. This is further emphasized by the fact that, even in the unoccupied site, the occupation probability of the impurity electron is not zero due to the virtual transition, and this probability increases as the activation energy decreases. Then, 4f spin alignment in the unoccupied site increases further and so on. The applied field is replaced by the molecular field for the ferromagnetic ordering, and as the ferromagnetic ordering begins to appear, the activation energy decreases very rapidly with a drastic decreasing of the resistivity, and the main transport mechanism changes from the hopping type to the metallic-impurity band conduction discussed in Sec. A.

For the actual calculation, the simplest model for the single-phonon-assisted hopping conduction is used for  $C \ll 1$ ,

$$\sigma = (2\pi e^2 / \hbar \kappa T) \eta R_{\text{eff}}^2 N_h f(\Delta E / \kappa T) \sum_{i, j, \nu} w_0(i) \times \langle |w_{ij}|_{\nu}^2 \rangle_{\Delta} |g(\Delta)| N_{\nu}(|\Delta|), \quad (17)$$

in which  $\eta$  is the number of the effective n.n. divided by 3,  $R_{\text{eff}}$  the effective n.n. distance for the given path,  $N_h$  the effective number of unoccupied sites,  $f(x)$  is given approximately by

$$f(x) = 1 / (1 + c^{1/2} e^x), \quad (18)$$

$c$  is the degree of the compensation and  $\Delta E$  is the effective activation energy in the sense of Sec. IV.A,  $w_0(i)$  is the probability for the initial state of a typical pair of occupied and unoccupied impurity states excluding the local-potential effects,  $\langle |w_{ij}|_{\nu}^2 \rangle_{\Delta}$  is the square of the transition matrix from the initial state to the final state due to the electron- $\nu$ th-phonon interaction averaged on the equienergy surface of the  $\nu$ th phonon with the energy  $|\Delta|$ , in which  $\Delta = E_j - E_i$ ,

$$g(\Delta) = 1 / (e^{\Delta / \kappa T} - 1) \quad (19)$$

is the Bose distribution function allowing the negative  $\Delta$ , and  $N_{\nu}(|\Delta|)$  is the state density of the  $\nu$ th phonon with the energy  $|\Delta|$ .

The effect of local-potential fluctuation  $\Delta V$  along the path is included only in  $\Delta$  for simplicity. In the present model, the most important part for the transition matrix is the spin-dependent part. This is calculated as the following overlap integral between a molecule occupied by an impurity electron, of which the state is defined by  $|S_m, S_m^z, S_u, \pm, \xi\rangle$ , and a molecule without an impurity electron,  $|S_n, S_u, S_n^z, \xi\rangle$ , in which  $\pm$  indicates the parallel or antiparallel coupling of  $\delta$ , and  $\xi$  is the multiplicity among the states defined by  $S_u$ . For the spin-independent part, we simply assume that it is  $p$ -fold proportional to the phonon energy. It is a complicated problem to determine the most effective path for each temperature. Here, for simplicity, the high-temperature limit is used for this determination, and all effects are included in  $\Delta V$ .

When there is no magnetic field, the calculation is performed straightforwardly and the solid curve in Fig. 14 is obtained. The result scarcely depends on the choice of  $p$ . In this figure, the case of  $p=1$  and  $\Delta V=4J_1$  is given. The agreement with the experimental results is satisfactory.

In the case of an applied magnetic field, more assumptions are necessary to perform the calculation. Here, the following effective field is used for the unoccupied site:

$$H_{\text{eff}} = H_1 + 2\beta J_1 \langle \sigma \rangle, \quad (20)$$

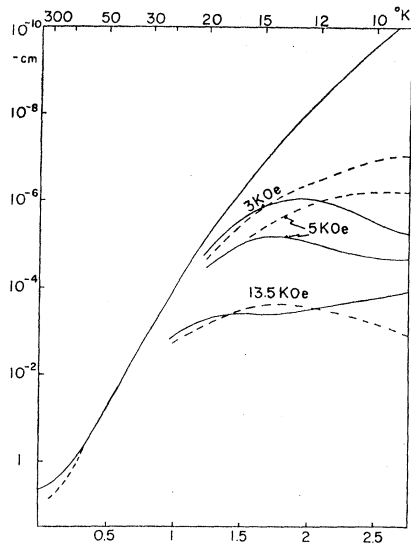


FIG. 14. Theoretical (solid lines) and experimental (dashed lines from Fig. 3) results for the resistivity of  $\text{Gd}_{0.01}\text{Eu}_{0.99}\text{Se}$  are shown. The exchange parameters are taken as  $J_1=25\kappa$ ,  $J_2=105\kappa$ ,  $T_{\text{eff}}=902\kappa$ , and  $J=1.14\kappa$  ( $J$  is determined from  $T_c=6^\circ\text{K}$ ). The experimental data for  $H=0$  are all on the theoretical line (solid line without assignment), except for room temperature.

in which  $H_1$  is the effective field on  $4f$  spins of the free  $\text{Eu}^{2+}$  defined by Eq. (9) and the second term comes from the  $s$ - $f$  exchange interaction due to the impurity electrons virtually transferred to the unoccupied site. The transferred probability  $\beta$  depends on both temperature and the magnetic field because it should increase as the effective activation energy from the occupied site to the unoccupied site decreases. In Fig. 14, a constant value  $\beta=0.2$  is used for simplicity. The agreement is good for the higher-temperature region. In the order of magnitude for the hopping conductivity at room temperature, the calculation from the simple model agrees well with the experimental value, in which the electron-phonon coupling constant is estimated from the mobility in the conduction band at room temperature obtained in Sec. II, and  $C^{-1}$  is assumed as 10.

The transport mechanism in the metallic impurity band has already been given.<sup>49</sup> Here, the effective number of the hole contributing to the metallic-impurity band conduction is estimated to be fairly small, less than 1% for 1% Gd alloy.

The detailed calculation in this section is given in Ref. 50.

## V. SUMMARY

A model for the band structure and various energy levels is given in Fig. 7, and the reason for the inadequacy of Cho's band model is given in the Appendix. In the present model the properties of the

optically active magnetic exciton are obtained from the anomalous optical phenomena.

The appearance of the giant spin molecule in the magnetic impurity state due to the  $s$ - $f$  exchange interaction is essential for the anomalous magnetic properties of the dilute  $\text{R}_x^{3+}\text{Eu}_{1-x}\text{X}$ . The very large initial increase of  $\Delta\theta$  is due to the first-order  $s$ - $f$  exchange interaction, and is different from the second-order effect in the usual ferromagnetic metals.

The transition from the hopping-type to the impurity-band conduction is also explained satisfactorily from the temperature-dependent activation energy due to the  $s$ - $f$  exchange interaction in the magnetic impurity state.

The model proposed by Callen<sup>51</sup> for the anomalous behavior of  $\Delta\theta$  is not acceptable because, first, very many valleys in his model are hard to expect from the usual band calculation in the present materials and, second, his model cannot explain the different behavior of  $\Delta\theta$  and  $\Delta T_c$ , together with the anomalous optical properties and the transport phenomena.

The spin-polaron<sup>52</sup> model for the anomalous transport properties is also not acceptable. This is similar to the small polaron expected in NiO, although from recent experiments the usual impurity conduction mechanisms are rather expected, and thus is the character of the conduction band. The mobility in the conduction band is, however, fairly large as discussed in Sec. II, and the anomalous properties should be attributed to the mechanism in the impurity band.

The present mechanisms and properties do not seem to be special for Eu-chalcogenide alloys but rather common for magnetic-semiconductor alloys. Actually, the recent experiments on  $\text{In}_x\text{Gd}_{1-x}\text{Cr}_2\text{Se}_4$  very likely suggest that the same mechanisms govern the anomalous properties in this material.<sup>53,54</sup>

## APPENDIX

The occupied  $4f$  levels should be in the band gap due to the following facts: (i) When  $\text{Na}^+$  or  $\text{K}^+$  replaces  $\text{Eu}^{2+}$  dilutely, an acceptor level should be formed in Cho's model and the system should become  $p$ -type semiconductor. While for the present model, the occupied  $4f$  levels have higher energy than the acceptor level, one electron moves from the Eu site to the Na site. Then the  $\text{Eu}^{3+}$  state appears instead of the acceptor level and the system persists as an insulator. The latter is consistent with the experiment.<sup>55</sup> It is also known that in these compounds  $\text{Eu}^{2+}$  vacancy is created in the crystal very easily. The situation is similar to the above case and then two  $\text{Eu}^{3+}$  are formed accompanied by an  $\text{Eu}^{2+}$  vacancy. This is the most important origin of the compensator in  $\text{R}_x^{3+}\text{Eu}_{1-x}\text{X}$ . (ii) In our model, the optical absorption edge should not change so much for various types of X because it is primarily due

to the intra-atomic  $4f-5d$  transition on  $\text{Eu}^{2+}$ . It should decrease gradually in wavelength as X changes from O to Te because the magnetic exciton has lowest energy in  $\text{EuO}$  due to the lowest potential energy of O among various X. This is actually the case in Fig. 5. While for Cho's model, the absorption edge is due to the interatomic transition from X to Eu, the completely opposite conclusion from Fig. 5 is obtained because the band gap should decrease as X changes from O to Te, as is shown by photoabsorption experiments on  $\text{SrX}$  and  $\text{BaX}$ .<sup>55</sup> (iii) The strong Faraday rotation and the large shift of the absorption spectrum at low temperature or under magnetic field are also not explained by Cho's model. The comparison of the absorption spectrums of  $\text{Eu}^{2+}\text{Te}$  and  $\text{Sr}^{2+}\text{Te}$ <sup>34</sup> is also naturally appreciated by the present model. Note that the electronic states of  $\text{Sr}^{2+}$  and  $\text{Ba}^{2+}$  are very similar to that of  $\text{Eu}^{2+}$ .

The conclusion that the bottom of the conduction band is of nondegenerated  $s$  character located at  $\Gamma_1$  is obtained, in the present stage, not from direct experiment but from the following knowledge given in Sec. III: (i) The mobility of the bottom of the conduction band is very large and this is inconsistent with the  $d$ -band model. Compare, for example, with the low mobility in the conduction band of  $\text{NiO}$  which is believed to be a  $3d$  band.<sup>56</sup> (ii) The exchange interaction between two impurity states separated moderately is negative and fairly large. This is consistent with the two-hydrogen model even in the magnitude, but contradicts the degenerate  $d$ -band model. (iii) The exchange interaction between the impurity electron and the  $4f$  electrons at the nearest neighbor  $\text{Eu}^{2+}$  is fairly smaller than that in the magnetic exciton but is consistent with  $I_{sf}$  in Table II.

## REFERENCES

Magnetic properties of pure compound:

- <sup>1</sup> B. T. Mattias, R. M. Bozorth, and J. H. Van Vleck, *Phys. Rev. Letters* **7**, 160 (1961).
  - <sup>2</sup> T. R. McGuire, B. E. Argyle, M. W. Shafer, and J. S. Smart, *J. Appl. Phys.* **34**, 1345 (1963); **35**, 984 (1964).
  - <sup>3</sup> U. Enz, J. F. Fast, S. Van Houten, and J. Smit, *Phillips Res. Rept.* **17**, 451 (1962).
  - <sup>4</sup> G. Busch, P. Schwob, and O. Vogt, *Phys. Letters* **20**, 602 (1966).
  - <sup>5</sup> P. Schwob and O. Vogt, *Phys. Letters* **22**, 374 (1966).
  - <sup>6</sup> G. Busch, P. Junod, P. Schwob, and O. Vogt, *Phys. Letters* **9**, 7 (1964).
  - <sup>7</sup> P. Junod and F. Levy, *Phys. Letters* **23**, 624 (1966).
  - <sup>8</sup> P. Schwob and O. Vogt, *Phys. Letters* **24A**, 242 (1967).
- Neutron diffraction:
- <sup>9</sup> N. G. Nersis, C. E. Olsen, and G. P. Arnold, *Phys. Rev.* **127**, 2101 (1962).
  - <sup>10</sup> S. J. Pickart and H. A. Alperin, *Bull. Am. Phys. Soc.* **10**, 32 (1965).
  - <sup>11</sup> J. Joenk, *Bull. Am. Phys. Soc.* **11**, 109 (1966).
  - <sup>12</sup> G. Will, S. J. Pickart, H. A. Alperin, and R. Nathans, *J. Phys. Chem. Solids* **24**, 1679 (1963).

Magnetic Resonance and Anisotropy:

- <sup>13</sup> S. H. Charap and E. L. Boyd, *Phys. Rev.* **133**, A811 (1964).
- <sup>14</sup> G. A. Uriana and R. L. Streever, *Phys. Letters* **17**, 205 (1965).

<sup>15</sup> G. B. Benedek, *Proc. Intern. Conf. Magnetism*, Nottingham, England, 1964, 97 (1965).

<sup>16</sup> S. von Molnar and A. W. Lawson, *Phys. Rev.* **139**, A1598 (1965).

<sup>17</sup> G. Busch, B. Natterer and H. R. Neukomn, *Phys. Letters* **23**, 190 (1966).

<sup>18</sup> J. F. Dillon Jr., and C. E. Olsen, *Phys. Rev.* **135**, A434 (1964).

<sup>19</sup> M. Miyata and B. E. Argyle, *Phys. Rev.* **157**, 448 (1967).

Heat capacity:

<sup>20</sup> C. F. Guerci, V. L. Moruzzi, and D. T. Teaney, *Bull. Am. Phys. Soc.* **9**, 225 (1964).

<sup>21</sup> V. L. Moruzzi and D. T. Teaney, *Solid State Commun.* **1**, 127 (1963).

<sup>22</sup> D. C. McCollin, Jr., and J. Callaway, *Phys. Rev. Letters* **9**, 376 (1962); *Phys. Rev.* **130**, 1741 (1963).

<sup>23</sup> G. Busch, P. Junod, R. G. Morris, J. Muheim, and W. Stutius, *Phys. Letters* **11**, 9 (1964).

Optical Data:

<sup>24</sup> G. Busch, P. Junod, M. Risi and O. Vogt, *Proc. Intern. Conf. Semiconductors*, Exeter, England, 1962, 727 (1962).

<sup>25</sup> G. Busch, P. Junod, and P. Wachter, *Phys. Letters* **12**, 11 (1964).

<sup>26</sup> G. Busch and P. Wachter, *Phys. Letters* **20**, 617 (1966).

<sup>27</sup> G. Busch, *J. Appl. Phys.* **38**, 1386 (1967).

<sup>28</sup> J. C. Suits and B. E. Argyle, *J. Appl. Phys.* **36**, 1251 (1965); *Phys. Rev. Letters* **14**, 687 (1965).

<sup>29</sup> B. E. Argyle, J. C. Suits, and M. J. Freiser, *Phys. Rev. Letters* **15**, 822 (1965); *J. Appl. Phys.* **37**, 1391 (1966).

<sup>30</sup> J. Muller and A. W. Lawson, *Phys. Letters* **24A**, 303 (1967).

Data for  $\text{Eu}_{1-x}\text{R}_x^{3+}\text{X}$ :

<sup>31</sup> J. C. Suits, *Bull. Am. Phys. Soc.* **8**, 381 (1963).

<sup>32</sup> F. Holtzberg, T. R. McGuire, S. Methfessel, and J. C. Suits, *Phys. Rev. Letters* **13**, 18 (1964); *Proc. Int. Conf. Magnetism*, Nottingham, England 1964, 470 (1965).

<sup>33</sup> S. Methfessel, *Z. Angew. Phys.* **18**, 414 (1965).

<sup>34</sup> F. Holtzberg, T. R. McGuire, and S. Methfessel, *J. Appl. Phys.* **37**, 976 (1966).

<sup>35</sup> T. R. McGuire, M. W. Shafer, and W. Palmer, *Proc. Intern. Conf. Magnetism*, Nottingham, England, 1964, 97 (1965).

<sup>36</sup> R. R. Heikes and C. W. Chen, *Physics* **1**, 159 (1964).

<sup>37</sup> S. von Molnar and S. Methfessel, *J. Appl. Phys.* **38**, 959 (1967).

<sup>38</sup> H. B. Callen and E. Callen, *Phys. Rev.* **136**, 1675 (1964).

<sup>39</sup> S. J. Cho, *Phys. Rev.* **157**, 632 (1967).

<sup>40</sup> H. N. Russell, W. Albertson, and D. N. Davis, *Phys. Rev.* **60**, 641 (1941).

<sup>41</sup> W. R. Callahan, *J. Opt. Soc. Am.* **53**, 695 (1963).

<sup>42</sup> A. Yanase and T. Kasuya, *J. Phys. Soc. Japan* **25**, No. 4 (1968).

<sup>43</sup> H. Y. Fan, *Solid State Phys.* **1**, 284 (1955).

<sup>44</sup> V. L. Moruzzi, D. T. Teaney and B. J. C. van der Hoeven, *Jr.*, *IBM Res. Rept.* RC-2008, 1968 (unpublished).

<sup>45</sup> M. W. Shafer and T. R. McGuire, *J. Appl. Phys.* **39**, 588 (1968).

<sup>46</sup> T. Kasuya and S. Koide, *J. Phys. Soc. Japan* **13**, 1287 (1958); *N. F. Mott and W. D. Twose, Advan. Phys.* **10**, 107 (1961).

<sup>47</sup> H. Fritzsche, *J. Phys. Chem. Solids* **6**, 69 (1958).

<sup>48</sup> K. Takeyama, *J. Phys. Soc. Japan* **23**, 1013 (1967). For further information, see the references therein.

<sup>49</sup> T. Kasuya, *J. Phys. Soc. Japan* **13**, 1096 (1958); *T. Matsumbara and Y. Toyozawa, Progr. Theoret. Phys. (Kyoto)* **26**, 739 (1961).

<sup>50</sup> A. Yanase and T. Kasuya, *J. Phys. Soc. Japan* (to be published).

<sup>51</sup> E. Callen, *J. Appl. Phys.* **39**, 519 (1968).

<sup>52</sup> S. von Molnar, *J. Appl. Phys.* **39**, 899 (1968).

<sup>53</sup> H. W. Lehmann, *Phys. Rev.* **163**, 488 (1967).

<sup>54</sup> C. Haas, A. M. J. G. Van Run, P. F. Bongers, and W. Albers, *Solid State Commun.* **5**, 657 (1967).

<sup>55</sup> R. J. Zollweg, *Phys. Rev.* **111**, 113 (1958).

<sup>56</sup> A. J. Bosman and C. Crevecoeur, *Phys. Rev.* **144**, 763 (1966).

## Discussion of Kasuya and Yanase's Paper

E. CALLEN (U. S. Naval Ordnance Labs.): I wonder if I can precis a talk which I am going to give next Wednesday at the

Berkeley meeting, on the temperature dependence of the absorption edge of the cadmium chromium chalcogenide spinels and of the europium chalcogenides. For definiteness consider EuS. The gap width  $E_g$  is about 1.51 eV at 0°K, increases—at first slowly with increasing  $T$  and, near  $T_c$ , more rapidly—to about 1.66 eV at  $T_c$ , and then has a long tail above the Curie temperature. At  $2T_c$  the gap width is about 1.69 eV, so the entire increase in  $E_g$  is about 0.2 eV, or more than 10%. The strongest  $T$  dependence, and magnetic field dependence are near  $T_c$ . All this can be understood, both in the europium chalcogenides and in the cadmium chromium spinels in a simple way, if one considers that the energy difference between conduction and valence bands in the presence of a strain is the gap width with no strain plus a deformation potential  $\Xi$  times the volume strain  $\epsilon$ :

$$E_g(\epsilon) = E_g(0) + \Xi\epsilon. \quad (1)$$

Now we require  $\epsilon$ . The Hamiltonian of the spin system is

$$H = H_n - \epsilon \sum_{ij} D_{ij} \mathbf{S}_i \cdot \mathbf{S}_j + \frac{1}{2} C \epsilon^2. \quad (2)$$

The first term is the ordinary Heisenberg energy, the last term is the elastic energy, and the second term is the magnetoelastic energy. Clearly,  $-D$  is the change in the exchange constant with strain. The first two terms are just a Taylor's series expansion

$$H_n(\epsilon) \cong |J_0 + (\partial J / \partial \epsilon) \epsilon| (\mathbf{S}_i \cdot \mathbf{S}_j). \quad (3)$$

From Eq. (2), the first-order free energy is calculated and minimized with respect to strain, yielding

$$\epsilon = C^{-1} \sum_{ij} D_{ij} \langle \mathbf{S}_i \cdot \mathbf{S}_j \rangle_0. \quad (4)$$

Thus, from Eq. (4) and Eq. (1), the gap width depends upon  $T$  and  $H$  through the scalar correlation function  $\langle \mathbf{S}_i \cdot \mathbf{S}_j \rangle$ . This quantity can be calculated, either by Green's functions, which is hard, or by a cluster theory, which is much easier, and it has exactly the character observed in the absorption-edge experiments. Furthermore its magnitude is right. The integrated magnetic contribution to the thermal expansion, which is the magnetic volume strain, is  $10^{-2}$  in both EuO and in nickel metal—this is its usual size. A canonical deformation potential is 10 eV. Thus the expected total gap-width shift is roughly  $\epsilon \Xi \cong 0.1$  eV compared to the observed 0.2 eV.

S. METHESSEL (I.B.M. Research): There was one curve for the resistivity as a function of temperature or magnetic order for 5% gadolinium in Eu selenide. This sample has about  $10^{19}$  carriers. The temperature dependence of the resistivity for  $10^{20}$  carriers agrees surprisingly well with the critical scattering theory of Friedel and de Gennes. This is a theory which applies to Bloch electrons scattered by the magnetic disorder as a small

perturbation. From here one goes continuously to samples which have a carrier concentration reduced by about two orders of magnitude. These samples become insulating at the magnetic Curie temperature, which implies extremely strong interactions of the electrons with the spin order. On the other hand, tunneling experiments on pure, insulating materials have been performed by Esaki, Stiles, and von Molnar [Phys. Rev. Letters **19**, 852 (1967)] which show that the bottom of the conduction band depends on the magnetic spin order. Here the electrons come from aluminum electrodes and tunnel into the empty conduction band. The I-V characteristics shift with the magnetic order by an amount approximately equal to the activation energies for the trapping of the carrier. There is, consequently, some temptation to start the problem from the free-electron side. Then one must replace the interaction of the electron with phonons or charge fluctuations by the interaction of electrons with spin fluctuations. It would appear possible that electrons get trapped magnetically in some spin or magnon fluctuation.

T. KASUYA: I believe that, if the experiments referred to here are correct, only the present model with the ideas of the magnetic-exciton and the magnetic-impurity state of the giant spin molecule can explain the whole anomalous properties consistently both qualitatively and quantitatively. Other proposed models may explain some of the properties but fail to explain others consistently. The tunneling experiments by Esaki *et al.*, also shows the decreasing of the bottom of the conduction band due to the  $s$ - $f$  exchange interaction. A rough estimation seems to be favorable to  $I_{sf}$  rather than  $I_{sj}$  consistent to the present model. Unfortunately, however, there seems to be much ambiguity [L. Esaki, P. J. Stiles, and S. von Molnar, Phys. Rev. Letters **19**, 852 (1967)].

*Note Added in Proof:*

(1) The mechanism for the red shift mentioned by Callen is too small in magnitude and gives the wrong sign because we know from the pressure experiment that the ferromagnetic exchange increases with decreasing lattice constant and thus the lattice shrinks in the ferromagnetic region and also the absorption edge energy increases with decreasing temperature. Furthermore his assignment on the absorption edge as due to the valence-conduction bands transition is I believe, to be established as wrong (see this Appendix).

(2) I think that the anomalous resistivity of 5% Gd-EuSe in Fig. 3(b) may be due to the hopping mechanism described here. Recent experiments by von Molnar on a better 5% Gd-EuS single crystal show the resistivity to be more than two orders of magnitude smaller than that in Fig. 3(b) and indicate that a well-defined conduction band begins to coexist with the localized impurity levels and band. The whole story on this sample is completely agreeable with our model and calculation described here [S. von Molnar and T. Kasuya (to be published)].